Evaluation of Enhanced Frame-Dragging in the Vicinity of a Rotating Niobium Superconductor, Liquid Helium and a Helium Superfluid

M. Tajmar

Department of Aerospace Engineering and Physics, KAIST, Daejeon, Republic of Korea
and
Department of Aerospace Engineering, University of Applied Sciences, Wiener Neustadt, Austria

E-mail: `martin.tajmar@kaist.ac.kr`

Abstract.
Tajmar and de Matos predicted that rotating superconductors or superfluids might produce large non-classical frame-dragging fields in order to explain a reported Cooper-pair mass anomaly in niobium. Also anomalous gyroscope signals close to the measurement resolution in the proximity of rotating superconductors or liquid helium were reported while trying to investigate this theoretical concept. Based on lessons from various setups, we succeeded in building an experimental facility that allowed us to rotate a niobium superconductor, liquid helium, superfluid helium and low temperature matter with high accelerations at high speed exceeding all previous efforts. A military-grade SRS-1000 gyroscope at close proximity in different locations was used to measure any anomalous frame-dragging-like fields. No such anomalies were found within three times the noise level of our setup ($\pm 5 \times 10^{-8}$ rad/s). Measurements with an electric motor at speeds up to 5000 RPM enabled us to set low boundaries for any coupling or frame-dragging-like effect outside of a rotating niobium superconductor or liquid helium to 4×10^{-11} and for superfluids to 3×10^{-10}. Due to the high speeds used, these results are up to two orders of magnitude below any previous result.

PACS numbers: 74.25.Ld, 67.25.D-, 04.80.Cc

1. Introduction

Frame dragging is a phenomenon in general relativity that causes rotating matter to drag space-time in its vicinity. According to Einstein's theory, this effect is so weak that it required astronomical observations and precision tests with satellites to detect it [1]. Recently, Tajmar and de Matos [2, 3, 4, 5] predicted that rotating superconductors or superfluids might produce much larger non-classical frame-dragging fields in order to explain a reported Cooper-pair mass anomaly in niobium [6, 7] which still remains unsolved at present [8]. Other theoretical concepts were proposed supporting this conjecture [9, 10, 11]. Recently, McCulloch proposed that such frame-dragging-like fields may be linked to the Pioneer anomaly [12]. Moreover, it was shown, that such fields would be of great technological interest as they could enable the creation of artificial gravitational fields to enable e.g. microgravity research in an Earth-based laboratory [13].

Since 2003, several experiments have been performed at the Austrian Institute of Technology (AIT) [14, 15, 16, 17, 18] to detect greatly enhanced frame-dragging fields using accelerometers (dismissed early on due to high vibration sensitivity) and fiber-optic gyroscopes in close vicinity to rotating matter at low temperature including steel, aluminum, Teflon, high- and low T_c superconductors, liquid and superfluid helium. Initially, the sensors were mounted inside the cryostat inside a separate vacuum chamber, which provided the necessary thermal isolation to operate them at 25 °C. This chamber with the sensors was fixed with stainless steel bars to the ceiling of the laboratory to remain fixed during the tests. When a ring sample cooled with liquid helium was rotated below the sensors, the gyroscope indeed seemed to follow the rotating ring with a coupling factor (gyroscope signal / ring angular velocity) of about 10^{-8} mimicing a frame-dragging-like measurement. Also a parity violation was observed such that clockwise rotation yielded larger couping factors than counter-clockwise rotation. The signal apparently did not decay over the distance of our vacuum chamber and was independent within a factor of two of the ring material used. It only decayed with the temperature of the ring (or with the liquid helium level in the cryostat) such that only temperatures close to liquid helium did show an effect. Although the gyroscope signal was very small, its magnitude was some 18 orders of magnitude above classical predictions. Of course, this warranted further investigation into the nature of the signals that we measured.

Because magnetic or temperature drift effects were soon ruled out, our main concern was vibration due to the motor and from the expansion of the liquid helium into gas during rotation. Our setup was gradually adapted by using low-noise cryomotors directly below the ring, a military-grade gyroscope with higher resolution and less vibration sensitivity as well as trying to move the gyroscope outside the cryostat for optimal vibration isolation. This resulted in lower rotation speeds and also smaller anomalous signals with coupling factors now in the range of 10^{-9}.

Also Graham et al [19] attempted to measure enhanced frame-dragging from a

rotating lead disc at 4 K using the world's largest ring-laser gyro and failed to detect a signal within $1.7 \pm 3.8 \times 10^{-7}$ assuming a dipolar distribution, a sensitivity which is about two orders of magnitude worse than our design (their experimental values were re-assessed in [16]) and therefore could not rule out our anomalous gyroscope signals. Moulthrop [20] investigated frame-dragging-like signals from rotating superfluid helium and put an upper limit coupling-factor of 0.05 which is 7 orders of magnitude worse compared to our anomalies.

In order to finally settle the case, we built a new experiment, where the test sample inside the cryostat can be rotated at high speeds using an externally mounted motor. The gyroscope is mounted outside the cryostat, isolated from the ground, and attached to a structure that allows mounting it at different positions. Our latest setup allows us to rotate a niobium superconductor and a pot with liquid helium or superfluid helium at high speeds and accelerations in order to re-evaluate all theoretically predicted possibilities (source of effect due to superconductivity, superfluid helium or the liquid helium itself).

2. Experimental Setup

2.1. Overview

The main part of our experiment is a large custom-built cryostat made out of stainless steel (evacuated with MLI isolation) as shown in Fig. 1. The cryostat is mounted on a structure which allows tilting it along the Earth's north-south axis as we planned to tilt the cryostat in future experiments to investigate the influence of the Earth's spin. However, all experiments performed so far were done with the cryostat mounted vertically to our laboratory floor. Inside the cryostat is a pot made out of aluminum with a wall thickness of 3 mm, which can be filled with up with 1.71 L of liquid helium. Its outer and inner radii are 173 mm and 45 mm with a height of 98 mm. As shown in Fig. 2, the pot can only be filled through a ring shaped hole on the top and it has four fins that ensure that the liquid is homogenously rotating with the same velocity. The fins have a 5 mm gap with respect to the outer wall and the inner rotating axis in order to allow closed loops for rotating superfluids to create vortices. In addition, a niobium ring with a thickness of 10 mm, an outer diameter of 173 mm and an inner diameter of 77 mm is attached at the bottom of the pot and fixed with screws.

The pot is mechanically attached to the main axle, which is stabilized with three ball bearings and extends up to a flexible coupling that allows mounting any kind of external motor to it. The lower and the middle bearings were low-temperature bearings with solid MoS_2 lubricants made by KOYO. For our experiments, we used a compressed air motor (Düsterloh PMW 400 Z24) similar to one in our early experiments with maximum acceleration as well as a brushless servo motor (Torque Systems BNR3034). The axle also features an optical encoder to readout the speed as well as a sealing lip that was inserted during the superfluid measurements which required evacuation of the

chamber. Silicon diodes (Lakeshore DT-670B-SD) were placed on the niobium disc as well as at the top of the inner cylindrical surface of the pot (readout via a slip ring close to the optical encoder as it is rotating with the pot) and on two positions inside the cryostat to monitor the filling level of the liquid helium and the temperatures. Great care was taken for good thermal isolation using styropor isolation foam rings as well as protecting the liquid helium in the upper part of the cryostat from the rotating axle by a shielding tube to minimize heat and rotation sources and hence the transition of liquid into gaseous helium. The helium gas exhaust was directly connected to a tube that extended through the windows of the laboratory to not influence our equipment.

We used an OPTOLINK SRS-1000 fiber-optic-gyroscope, which is mounted on a support structure outside the cryostat allowing it to change its position and orientation all around the cryostat. In addition, a magnetic field sensor (Honeywell SS495A1), high resolution accelerometers (Colibrys SiFlex1500 and SiliconDesigns 1221) and temperature sensors are mounted together with the gyroscope. All sensors are encapsulated under a high permeability magnetic shield (permalloy) in order to reduce their magnetic sensitivity. The support structure was lifted off the laboratory floor by a stiff structure made out of wood that was connected to the ceiling of the laboratory as shown in Fig. 1b. A gap of about 5 cm ensured a good vibration isolation during rotation between the vibrating cryostat, which was fixed to the ground by screws and the actual gyro support structures. In addition, the gyro support structure was passively damped by rubber sheets between the gyro support and the wood structure. The gyroscope was moved along four positions during the experiment labeled Middle, Side, Off-Axis and Off-Axis 2 as shown in Fig. 3 in order to investigate a possible field distribution of the anomalous signals.

2.2. Sensitivity and Systematic Effects

Since we are trying to measure very small rotation rates, it is important to know the minimum rotation rate that can be resolved by the fiber-optic gyroscope. For the SRS-1000 gyroscope, the upper limit of the minimal measured rotation rate, caused by polarization nonreciprocity of a light source with a Gauss spectrum, is expressed as [21] [22]

$$\Omega_{min} \leq \frac{\lambda c p \epsilon}{DL} \sqrt{\frac{\lambda \sqrt{ln2} h L_p}{\pi \Delta \lambda}} \tag{1}$$

where $\lambda = 1.55 \times 10^{-6}$ m is the average wavelength of light, $\Delta\lambda = 50 \times 10^{-9}$ m is the width of the light spectrum, c is the speed of light in vacuum, $D = 150 \times 10^{-3}$ m is the diameter of the fiber coil, $L = 1070$ m is the length of the fiber coil, $h = 1 \times 10^{-6}$ m^{-1} is the polarization crosstalk of the fiber coil, $L_p = 2.5 \times 10^{-3}$ m is the beat length of the fiber coil, p is the residual degree of polarization of the light source and ϵ is the coefficient of the polarizer's extinction. For typical values of $p \approx 0.01$ and $\epsilon \approx 0.01$ (i.e. 40 db), Equ. 1 gives an upper limit of $\Omega_{min} \leq 4.1 \times 10^{-8}$ rad/s. This coincides with

the bias drift value specified for the SRS-1000. We also tested the gyroscope on a piezo-activated nano-rotation table [23] and could resolve velocity steps of 1×10^{-7} rad/s with an accuracy of 1.5×10^{-8} rad/s which is just below the theoretically predicted resolution upper limit. No asymmetry has been seen between clockwise or counter-clockwise gyro responses.

The magnetic sensitivity along the gyro's axis is 4.8 ± 10^{-3} rad/s/T. According to our Hall sensor mounted directly on the gyroscope, the magnetic field changes during rotation (influence from brushless servo motor and Barnett effect) were always less than $1 \ \mu$T. Therefore, the magnetic influence is about one order of magnitude below our minimum rotation rate resolution.

3. Experimental Results

3.1. Calibration Runs

Before going to liquid helium, the whole setup was first evaluated by filling the pot with liquid nitrogen (for a cold environment - but no superconductivity of the niobium ring or superfluidity) and then with Ethanol as a general electrically non-conducting fluid at room temperature.

All experiments were done using the same standardized speed profiles which last about 200 seconds. The profile is subdivided into 5 sectors with pre-defined time intervals: rest, acceleration, maximum speed, de-acceleration and rest. Each profile is performed in clockwise direction (spin vector points downwards) and in counter-clockwise direction. Random noise was reduced by applying a 200 pt digital moving average (DMA) filter to the gyro output and motor velocity. A sampling rate of 13 Hz ensured that the averaging window is always smaller than the maximum speed time interval of the profile. After the signal is acquired, it is normalized by subtracting the Earth's rotation offset. The noise was further reduced by signal averaging of at least 10 (up to more than 50) profiles for each test case which also increases the statistical significance of our results. For the pneumatic air motor, the optical encoder data was used for the applied angular velocity, whereas in case of the brushless servor motor, the encoder velocity was used. Both were calibrated using reflection stripes on the axle and an external speedmeter.

Fig. 4 plots the gyroscope response mounted at the middle position during the rotation of both test fluids. The gyroscope shows only noise within a boundary of $\pm 5 \times 10^{-8}$ rad/s which is close to the upper limit sensitivity and the bias drift. We should therefore consider this value as our noise limit in the further analysis.

3.2. Measurements with Electric Motor

We used the brushless servo motor in order to evaluate the gyroscope response to different speeds than rather only maximum speed as in our earlier measurements. Two sets of measurements were taken: one for liquid helium and one with superfluid He^4.

3.2.1. Liquid Helium The cryostat was filled with liquid helium and a series of measurements was taken with the maximum speed during our profile measurements varying from 1000 RPM (about 100 rad/s) up to 5000 RPM. At this temperature, also the niobium ring at the bottom of the cryostat was superconducting.

A summary of our measurements in shown in Fig. 5, where the average signal and standard deviation was evaluated during the maximum speed phase of our speed profile. Apart from the two last high speed points at 4000 and 5000 RPM (400 and 500 rad/s) in the counter-clockwise direction, all measurement data is within our noise limit of $\pm\, 5 \times 10^{-8}$ rad/s. The detailed plot of the 4000 RPM test run is shown in Fig. 6. The gyroscope signal during counter-clockwise rotation (negative velocities) does not fully follow the angular velocity profile, and its maximum signal is only about a factor of 3 above our gyroscope resolution.

A linear fit through the measurements in Fig. 5 sets a new limit for a possible coupling factor (or frame-dragging-like coupling) between the liquid helium/superconducting niobium and a gyroscope in close proximity as $1.9 \pm 4 \times 10^{-11}$, which is nearly two orders of magnitude below previous measurements [17].

3.2.2. Superfluid Helium We also performed test runs with superfluid helium by filling the cryostat with liquid helium with the sealing lip on the main axle and subsequently pumping on it. We could reach a temperature down to 1.8 K in our pot, well below helium's Lambda point at 2.17 K. The test runs were done at three maximum speeds ranging from 500, 750 to 1000 RPM, which is an order of magnitude higher than our previous superfluid helium measurement [18]. Above 1000 RPM, we could not keep the temperature below the Lambda point during rotation.

The summary plot is shown in Fig. 7 and shows a similar picture to the one obtained with the liquid helium only. The data points are mostly within our noise level with one exception in the clockwise direction at 750 RPM which is again about a factor of 3 above our gyroscope resolution. The detailed plot from this particular speed is shown in Fig. 8.

Also here we can perform a linear fit through the measurements in Fig. 7 and set a new limit for a possible coupling factor (or frame-dragging-like coupling) between the superfluid helium and a gyroscope in close proximity as $1.6 \pm 3 \times 10^{-10}$.

3.3. Measurements with Air Motor

We then performed measurements using the pneumatic air motor which provided very high accelerations and a maximum angular velocity of around 4300 RPM which is comparable to the highest speeds that we achieved with the electric motor. Moreover, it has no electromagnetic noise which may influence the gyroscope. On the other hand, only one fixed speed is possible, however, we performed measurements at different locations as outlined in Fig. 3.

Two summary plots in Fig. 9 and Fig. 10 respectively show the results from our air

motor measurement on all different positions for the liquid helium as well as for helium gas (summarizing temperatures from 6 Kelvin up to room temperature) which we were running as non-liquid helium reference test runs. Whereas the helium gas reference measurements with error bars are really all within our noise limit of $\pm\, 5 \times 10^{-8}$ rad/s, the offset positions for the liquid helium case appear to show some room for anomalous signals. However, also here the maximum anomalous signal strengths are within 3 times our noise level which is not sufficient. Moreover, the anomalous signal is not consistent as for the Off-Axis position it's positive and for the Off-Axis 2 position it's negative. A similar sign would have been expected for any frame-dragging-like field at these two locations due to rotational symmetry. Detailed plots for all gyro positions during the liquid helium test runs are shown in Fig. 11 and Fig. 12 respectively.

4. Discussion and Conclusion

Our latest setup enabled us to perform high acceleration and high angular rotation of a niobium superconductor, liquid and superfluid helium together with a military-grade fiber-optic gyroscope mounted outside the cryostat and isolated from vibration. No anomalous signals were found up to within 3 times the noise level of our gyroscope ($\pm\, 5 \times 10^{-8}$ rad/s) which puts new bounds on any coupling or frame-dragging-like effect from superconductors, superfluids or low temperature matter. In addition, our accelerometers (mounted in tangential, radial and vertical direction) did not record any anomalous result within a noise band of ± 10 μg.

Our electric motor measurements at different speeds enabled setting very low standard deviation boundaries for external coupling effects (space-time like dragging of rotating matter) for superconductors and liquid helium to 4×10^{-11} and for superfluids to 3×10^{-10} outside of their boundaries. This is orders of magnitude below both previous theoretical predictions and measurements. A short comparison is given as follows:

- We speculated earlier that a frame-dragging-like field could account for a reported Cooper-pair mass anomaly in niobium. A coupling factor in the order of magnitude of 10^{-4} was predicted [3] in this case. In accordance with our previous measurements, such a possibility can be ruled out by some 7 orders of magnitude.

- Another prediction was that superfluid helium may produce frame-dragging-like fields with an even higher coupling factor in the order of unity [3]. Although Moulthrop [20] already ruled out a coupling factor down to 0.05, we can rule out such a possibility by some 10 orders of magnitude.

- All previous measurements which were performed outside the cryostat (Setup C [17] and Setup D [18]) recorded anomalous signals up to 1.5×10^{-7} rad/s similar to the maximum signals that we have seen in the present tests. However, the tests in this paper were performed at nearly 50 times the speed compared to our previous setups. Since the anomalous signals did not increase at higher speeds, they are most probably noise and data analysis artifacts.

   Although conclusions can be drawn for all results obtained previously and now outside the cryostat, an explanation for the large anomalous signals with up to 1.4×10^{-5} rad/s reported from gyroscopes inside the cryostat (Setup A and B in [17]) is still missing. Our results, however, suggest, that the liquid helium expansion during rotation created an acoustic noise environment that may have influenced the gyroscopes. This needs to be confirmed by future measurements.

   This leaves the following conclusions:

- Since our earlier speculation of non-classical frame-dragging fields from superconductors and superfluids can be ruled out, the starting point of the reported Cooper-pair mass anomaly in niobium is still not solved. That leaves the possibility for a weak-equivalence-principle (WEP) violation of Cooper-pairs or an unknown experimental error that was not accounted for in the setup from Tate et al [6, 7]. Both possibilities should be pursued and first theoretical concepts [24] as well as experimental assessments for WEP violation in superconductors [25] have been reported in the meantime. Tate's experiment should be repeated in order to further investigate the Cooper-pair mass anomaly.

- Replication attempts of our frame-dragging experiment should concentrate on our earlier Setup A and B [17] with the gyroscope embedded around a cold environment in order to either confirm them or identify the error source. Recent theoretical work points to the necessity of a cold environment to measure the effect [12].

Acknowledgement

References

[1] I. Ciufolini and E. C. Pavlis. A confirmation of the general relativistic prediction of the lensethirring effect. *Nature*, 331:958, 2004.

[2] M. Tajmar and C. J. de Matos. Gravitomagnetic field of a rotating superconductor and of a rotating superfluid. *Physica C*, 385(4):551–55, 2003.

[3] M. Tajmar and C. J. de Matos. Extended analysis of gravitomagnetic fields in rotating superconductors and superfluids. *Physica C*, 420(1-2):56–60, 2005.

[4] C. J. de Matos and M. Tajmar. Gravitomagnetic london moment and the graviton mass inside a superconductor. *Physica C*, 432(3-4):167–172, 2005.

[5] M. Tajmar and C. J. de Matos. Gravitomagnetic fields in rotating superconductors to solve tates cooper pair mass anomaly. volume 813 of *AIP Conf. Proc.*, pages 1415–1420, 2007.

[6] J. Tate, B. Cabrera, S. B. Felch, and J. T. Anderson. Precise determination of the cooper-pair mass. *Phys. Rev. Lett.*, 62:845–848, 1989.

[7] J. Tate, B. Cabrera, S. B. Felch, and J. T. Anderson. Determination of the cooper-pair mass in niobium. *Phys. Rev. B*, 42:7885–7893, 1990.

[8] Y. Jiang and M. Liu. Rotating superconductors and the london moment: Thermodynamics versus microscopics. *Phys. Rev. B*, 63:184506, 2001.

[9] R. Y. Chiao. Interference and inertia - a superfluid helium interferometer using an internally porous powder. *Phys. Rev. B*, 25(3):1655–1662, 1982.

[10] D. Brandt, D. J. Raine, and G. W. Fraser. Massive spin-1 gravity and the gravitational flux quantum. *Phys. Lett. A*, 372(14), 2008.

[11] J. Hauser and W. Droescher. Emerging physics for novel field propulsion science. volume 1208 of *AIP Conf. Proc.*, pages 168–185, 2010.

[12] M. E. McCulloch. Can the tajmar effect be explained using a modification of inertia? *Europhys. Lett.*, 89:19001, 2010.

[13] M. Tajmar. Homopolar artificial gravity generator based on frame-dragging. *Acta Astronaut.*, 66(9-10):1297–1301, 2010.

[14] M. Tajmar, F. Plesescu, K. Marhold, and C. J. de Matos. Experimental detection of the gravitomagnetic london moment. arxiv:gr-qc/0603033, 2006.

[15] M. Tajmar, F. Plesescu, B. Seifert, and K. Marhold. Measurement of gravitomagnetic and acceleration fields around rotating superconductors. volume 880 of *AIP Conf. Proc.*, pages 1071–1082, 2007.

[16] M. Tajmar, F. Plesescu, B. Seifert, R. Schnitzer, and I. Vasiljevich. Investigation of frame-dragging-like signals from spinning superconductors using laser gyroscopes. volume 969 of *AIP Conf. Proc.*, pages 1080–1090, 2009.

[17] M. Tajmar, F. Plesescu, and B. Seifert. Anomalous fiber optic gyroscope signals observed above spinning rings at low temperature. *J. Phys.: Conf. Ser.*, 150:032101, 2009.

[18] M. Tajmar and F. Plesescu. Fiber-optic-gyroscope measurements close to rotating liquid helium. volume 1208 of *AIP Conf. Proc.*, pages 220–226, 2010.

[19] R. D. Graham, R. B. Hurst, R. J. Thirkettle, C. H. Rowe, and P. H. Butler. Experiment to detect frame dragging in a lead superconductor. *Physica C*, 468(5):383–387, 2008.

[20] A. A. Moulthrop. *Tests of Macroscopic Wave Function Theories of He II*. PhD thesis, University of California, Berkeley, 1984.

[21] V. E. Prilutskii, V. G. Ponomarev, V. G. Marchuk, M. A. Fenyuk, Yu. N. Korkishko, V. A. Fedorov, S. M. Kostritskii, E. M. Paderin, and A. I. Zuev. Interferometric closed-loop fiber optic gyrocopes with linear output. Proceedings of the the 5th Pacific Rim Conference on Lasers and Electro-Optics, 2003.

[22] V. A. Fedorov. Personal communication, 2009.

[23] M. Tajmar, F. Plesescu, and B. Seifert. Precision angular velocity response of a fiber-optic gyroscope using a piezo nano-rotation table. *Meas. Sci. Technol.*, 20:027002, 2009.

[24] C. J. de Matos. Physical vacuum in superconductors. *J Supercond Nov Magn*, 23:1443–1453, 2010.

[25] M. Tajmar, F. Plesescu, and B. Seifert. Measuring the dependence of weight on temperature in the low temperature regime using a magnetic suspension balance. *Meas. Sci. Technol.*, 21:015111, 2010.
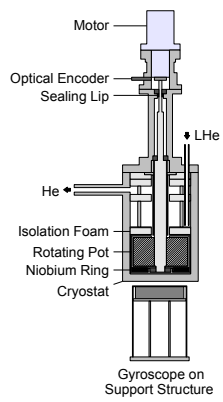
(a) Detailed Section
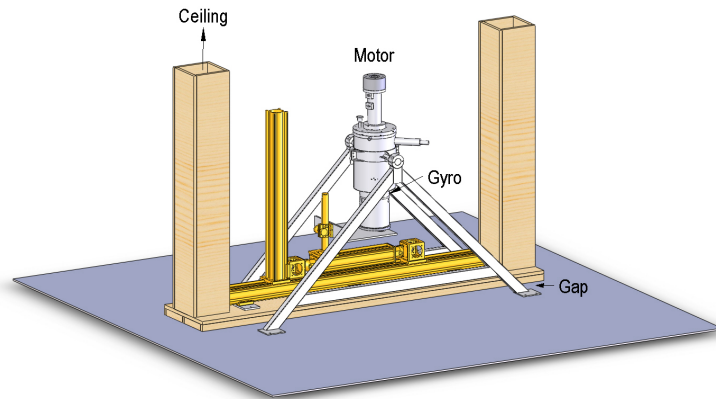
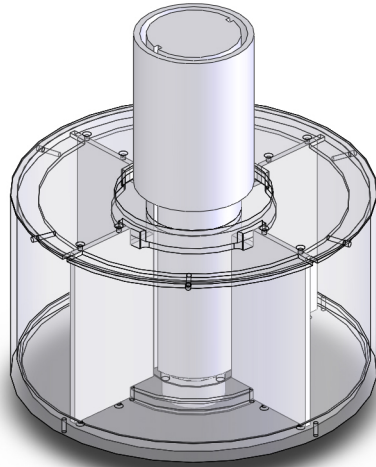(b) Overall Experimental Setup

Figure 1: Experimental Setup

Figure 2: Rotating Pot with Fins (Outer Walls are Transparent)
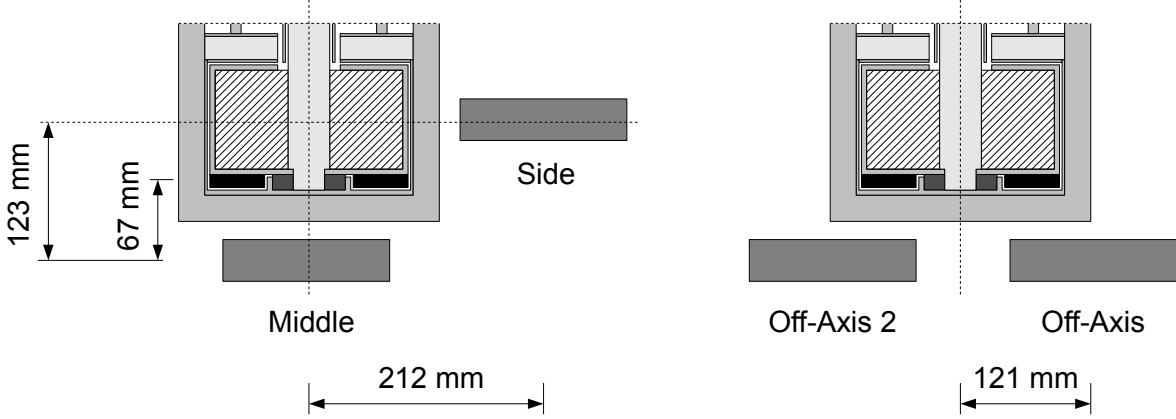
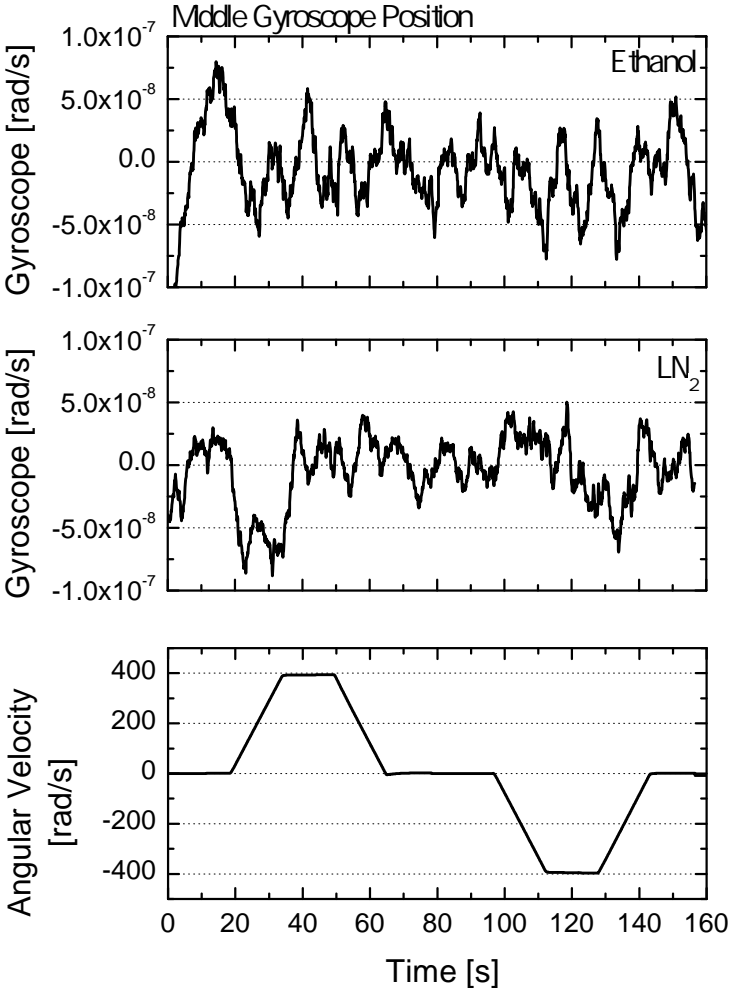Figure 3: Gyroscope Positions

Figure 4: Calibration Measurements with Ethanol and Liquid Nitrogen: Gyroscope Output (Middle Position) and Applied Angular Velocity
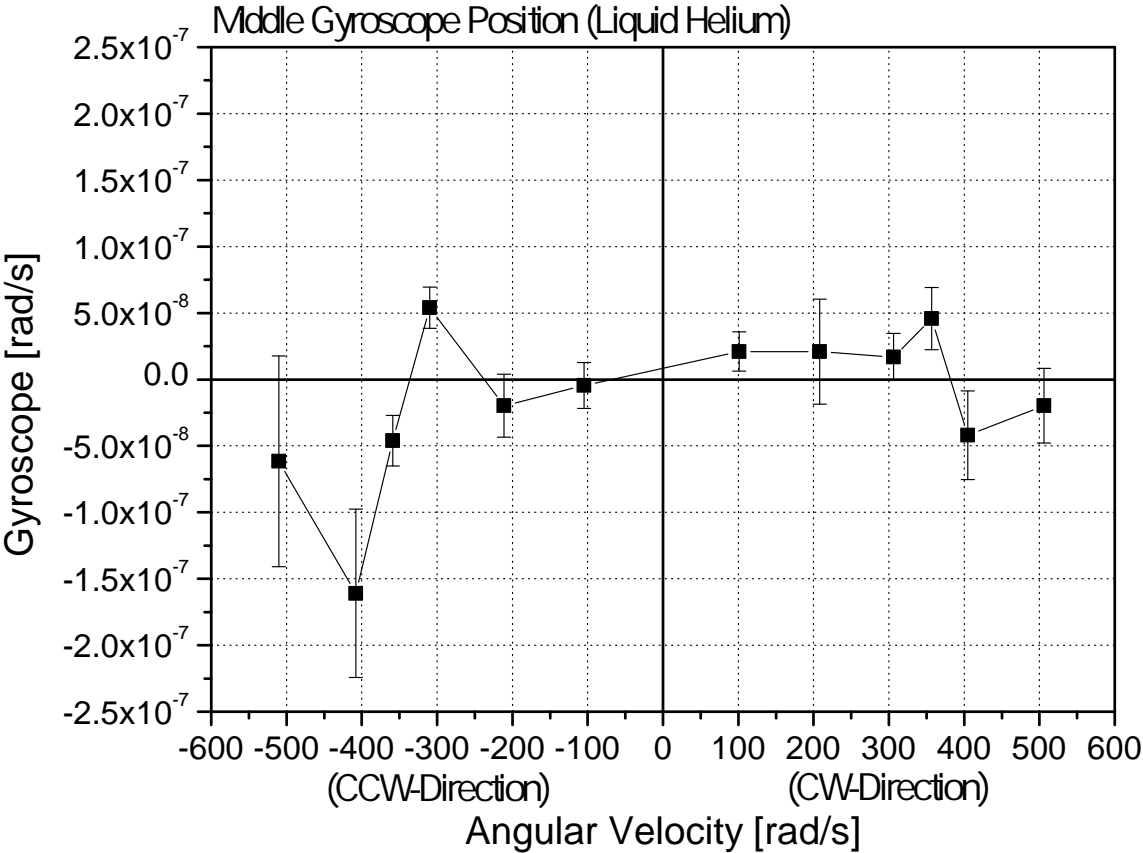
Figure 5: Liquid Helium Measurement with Electric Motor: Gyroscope Output (Middle Position) versus Applied Angular Velocity
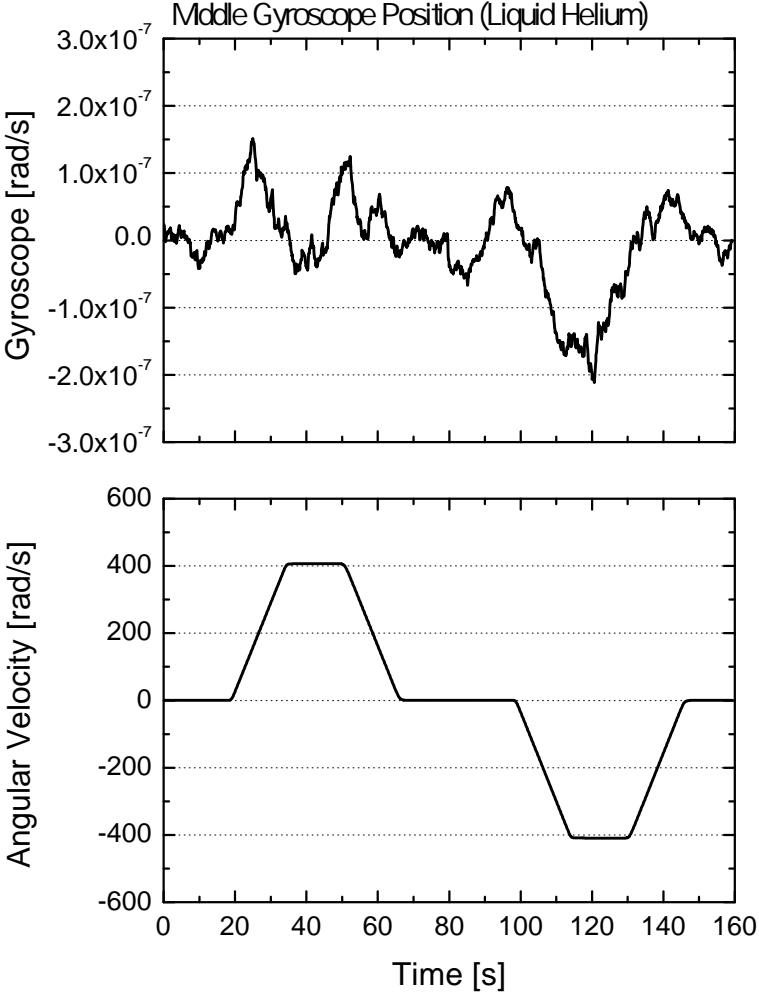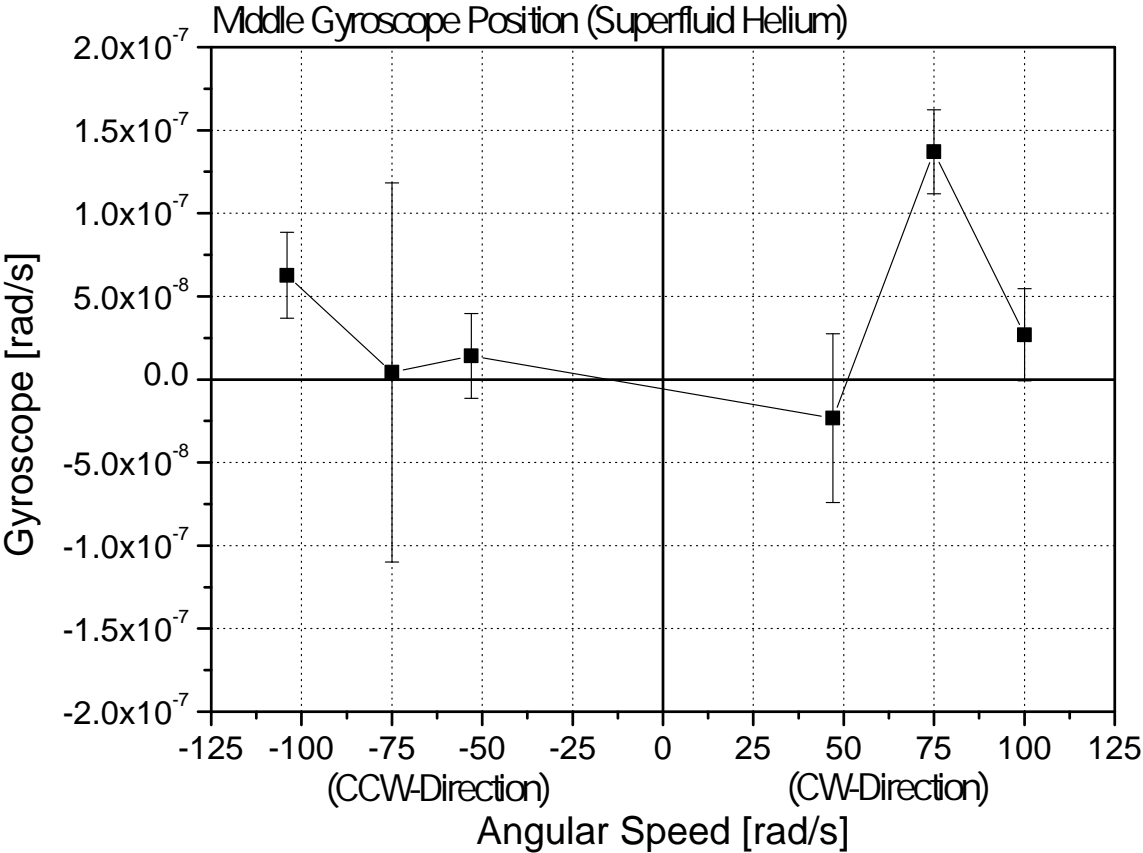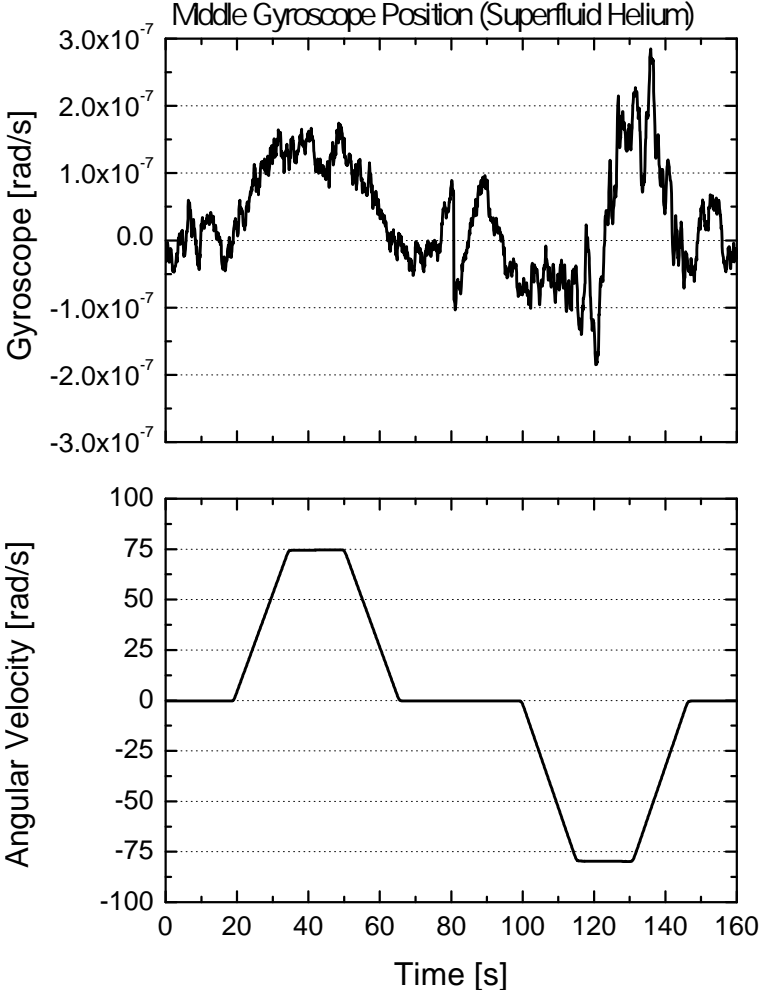
Figure 6: Liquid Helium Measurement Example at 4000 RPM: Gyroscope Output (Middle Position) versus Applied Angular Velocity
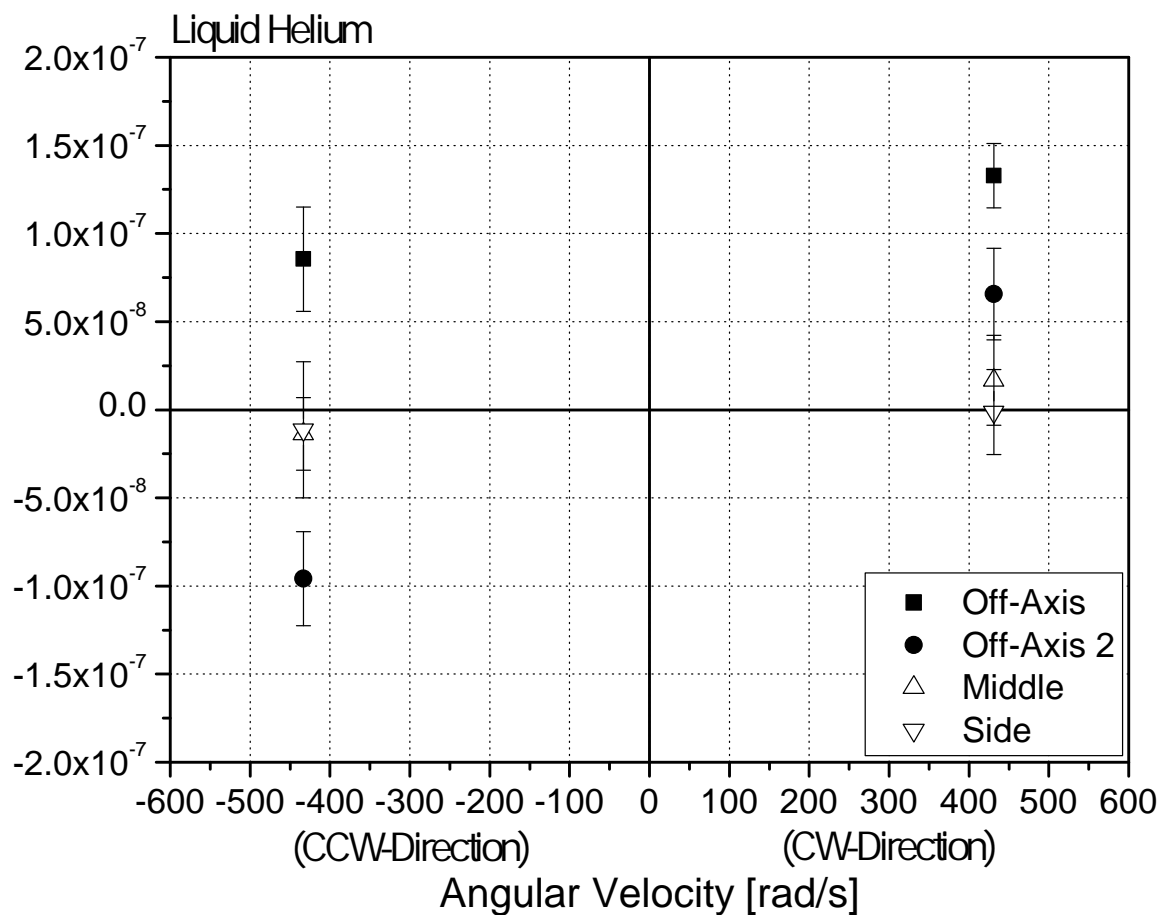
Figure 7: Superfluid Helium Measurement with Electric Motor: Gyroscope Output (Middle Position) versus Applied Angular Velocity

Figure 8: Superfluid Helium Measurement Example at 750 RPM: Gyroscope Output (Middle Position) versus Applied Angular Velocity

Figure 9: Liquid Helium Measurements with Air Motor: Gyroscope Output at Different Positions versus Applied Angular Velocity
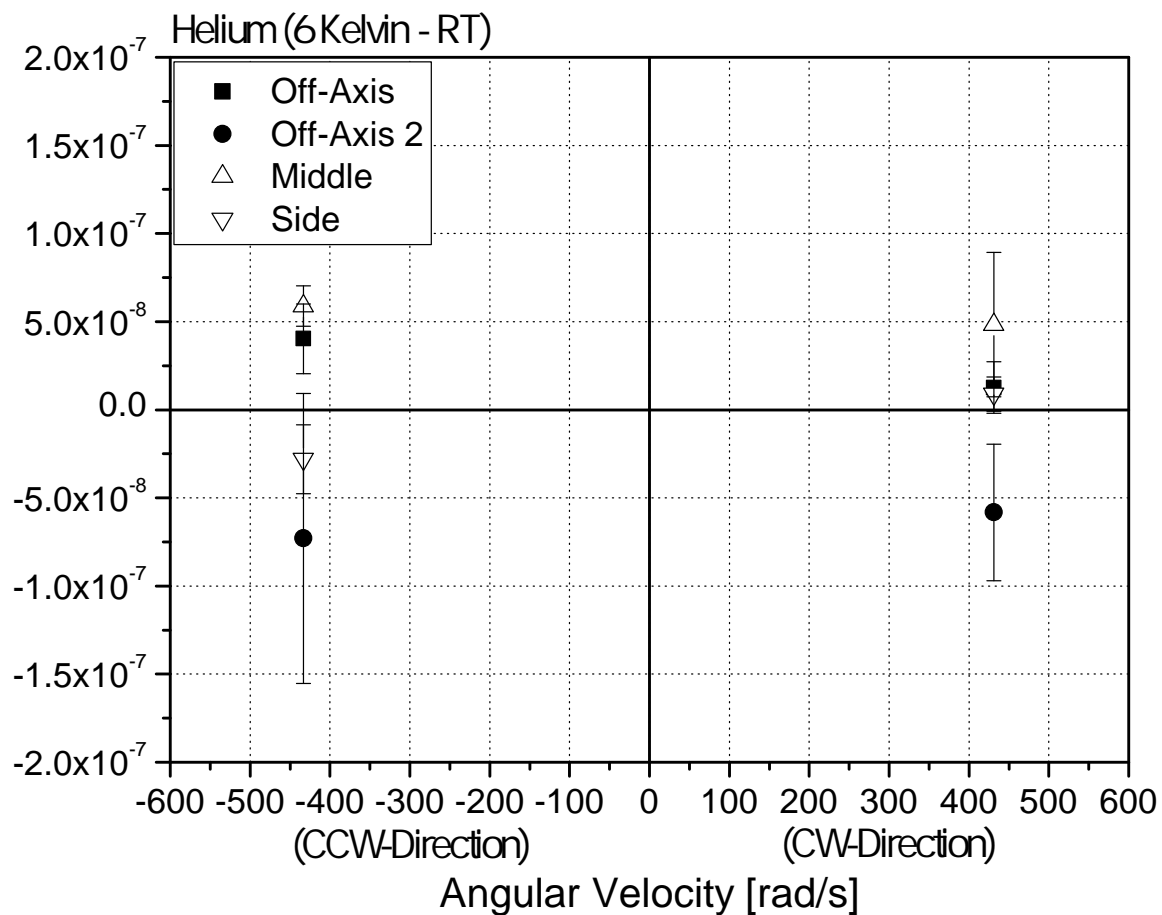
Figure 10: Helium Gas Measurements with Air Motor (Reference): Gyroscope Output at Different Positions versus Applied Angular Velocity
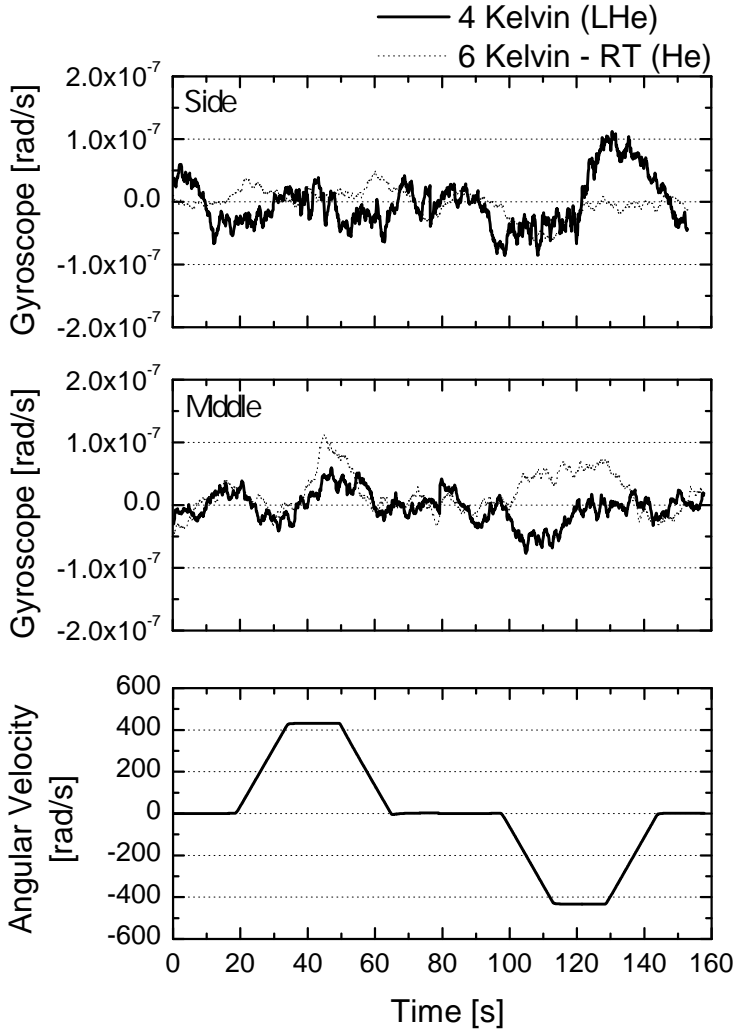
Figure 11: Liquid Helium Measurements with Air Motor: Gyroscope Output at Middle and Side Position versus Applied Angular Velocity
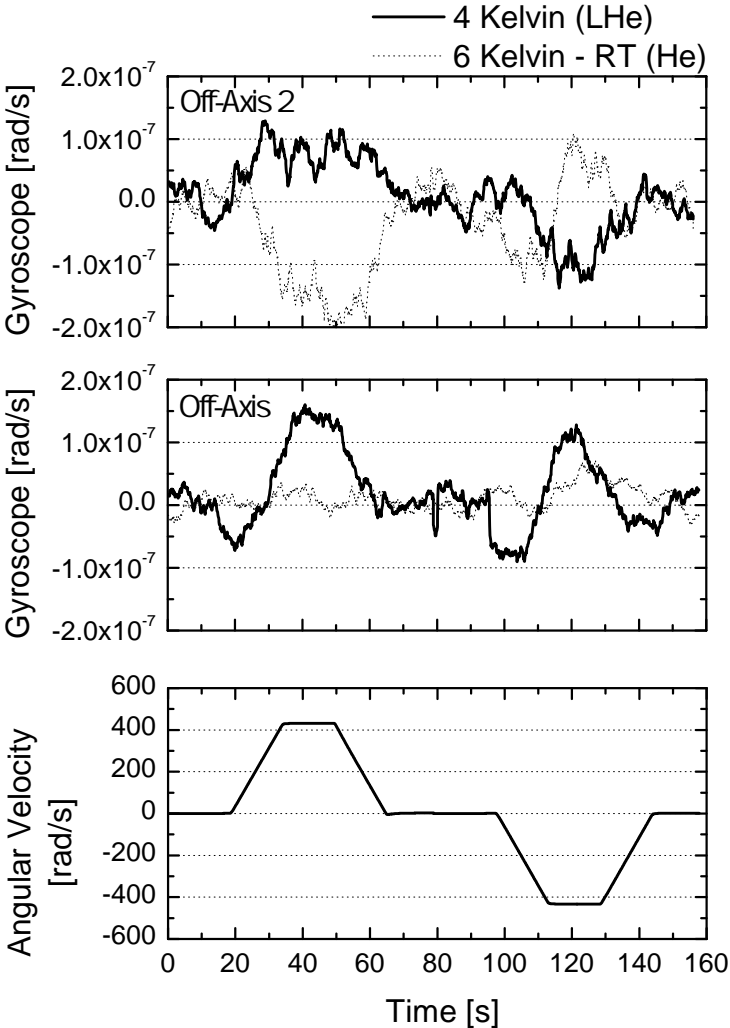
Figure 12: Liquid Helium Measurements with Air Motor: Gyroscope Output at Offset Positions versus Applied Angular Velocity